University of Kentucky
UKnowledge

Theses and Dissertations--Earth and Environmental Sciences

Earth and Environmental Sciences

2016

DENALI IN A BOX: ANALOG EXPERIMENTS MODELED AFTER A NATURAL SETTING PROVIDE INSIGHT ON GENTLE RESTRAINING BEND DEFORMATION

Anne M. Fendick
University of Kentucky, anne.fendick@uky.edu
Digital Object Identifier: https://doi.org/10.13023/ETD.2016.529

Right click to open a feedback form in a new tab to let us know how this document benefits you.

Recommended Citation

Fendick, Anne M., "DENALI IN A BOX: ANALOG EXPERIMENTS MODELED AFTER A NATURAL SETTING PROVIDE INSIGHT ON GENTLE RESTRAINING BEND DEFORMATION" (2016). *Theses and Dissertations--Earth and Environmental Sciences*. 45.
https://uknowledge.uky.edu/ees_etds/45

This Master's Thesis is brought to you for free and open access by the Earth and Environmental Sciences at UKnowledge. It has been accepted for inclusion in Theses and Dissertations--Earth and Environmental Sciences by an authorized administrator of UKnowledge. For more information, please contact UKnowledge@lsv.uky.edu.

STUDENT AGREEMENT:

I represent that my thesis or dissertation and abstract are my original work. Proper attribution has been given to all outside sources. I understand that I am solely responsible for obtaining any needed copyright permissions. I have obtained needed written permission statement(s) from the owner(s) of each third-party copyrighted matter to be included in my work, allowing electronic distribution (if such use is not permitted by the fair use doctrine) which will be submitted to UKnowledge as Additional File.

I hereby grant to The University of Kentucky and its agents the irrevocable, non-exclusive, and royalty-free license to archive and make accessible my work in whole or in part in all forms of media, now or hereafter known. I agree that the document mentioned above may be made available immediately for worldwide access unless an embargo applies.

I retain all other ownership rights to the copyright of my work. I also retain the right to use in future works (such as articles or books) all or part of my work. I understand that I am free to register the copyright to my work.

REVIEW, APPROVAL AND ACCEPTANCE

The document mentioned above has been reviewed and accepted by the student's advisor, on behalf of the advisory committee, and by the Director of Graduate Studies (DGS), on behalf of the program; we verify that this is the final, approved version of the student's thesis including all changes required by the advisory committee. The undersigned agree to abide by the statements above.

Anne M. Fendick, Student

Dr. Sean Bemis, Major Professor

Dr. Ed Woolery, Director of Graduate Studies

DENALI IN A BOX: ANALOG EXPERIMENTS MODELED AFTER A NATURAL SETTING PROVIDE INSIGHT ON GENTLE RESTRAINING BEND DEFORMATION

THESIS

A thesis submitted in partial fulfillment of the
requirements for the degree of Master of Science in the
College of Arts and Sciences
at the University of Kentucky

By
Anne Margaret Fendick
Lexington, Kentucky

Director:
Dr. Sean P. Bemis, Assistant Professor of Earth and Environmental Sciences
Lexington, Kentucky
2016

ABSTRACT OF THESIS

DENALI IN A BOX: ANALOG EXPERIMENTS MODELED AFTER A NATURAL SETTING PROVIDE INSIGHT ON GENTLE RESTRAINING BEND DEFORMATION

The Mount McKinley restraining bend (MMRB) creates an ~18° left-step in the arcuate surface trace of the dextral Denali Fault in south-central Alaska. Despite being a large, crustal-scale fault, little is understood about the controls on deformation within the MMRB. Similarities between previous wet kaolin analog modeling and the MMRB suggest that the first-order deformation patterns may derive from similar mechanisms. We compare uplift patterns, localization of deformation, formation of new faults, and displacement fields from the analog model and the natural setting to assess the influence of different variables on the overall system. Despite strong rheological heterogeneity in the MMRB, this natural setting exhibits the same distribution of deformation across the restraining bend as the homogeneous analog model suggesting this first-order deformation patterns is independent of upper crustal heterogeneity. The active thrust faults of the MMRB are purely dip-slip, whereas the thrust faults formed in the model exhibit oblique slip. Conventional understanding suggests migrating restraining bends cannot produce high topography; we conclude that with a specific combination of geometry, slip rate, and migration rate, high topography is capable of forming within a migrating system.

KEYWORDS: Mount McKinley Restraining Bend, Analog Modeling, Denali, First-order Deformation

Anne M Fendick

December 11, 2016

DENALI IN A BOX: ANALOG EXPERIMENTS MODELED AFTER A NATURAL SETTING PROVIDE INSIGHT ON GENTLE RESTRAINING BEND DEFORMATION

By

Anne Margaret Fendick

Sean Bemis
Director of Thesis

Ed Woolery
Director of Graduate Studies

December 11, 2016

ACKNOWLEDGMENTS

I would like to thank my advisor, Dr. Sean Bemis, for his guidance throughout my thesis, as well as for his continued confidence in me during this process. My committee members, Drs. Ed Woolery and Dave Moecher, were also instrumental in my success. Without the analog modeling from Dr. Michele Cooke and her graduate student, Kevin Toeneboehn, this thesis truly would not have been possible. I would also like to thank Jeff Benowitz for his help with low-temperature thermochronology and for providing feedback on an abstract submission for the 2016 European Geosciences Union meeting in Vienna, Austria.

This project was funded by the National Science Foundation award EAR 1250461. The Brown-McFarlan fund of the University of Kentucky's Earth and Environmental Sciences department provided travel support to attend EGU in April 2016. Research support was provided by the Ferm fund, also a University of Kentucky Earth and Environmental Sciences fund, to attend a Midland Valley Move Suite training course.

CONTENTS

Acknowledgments iii
List of Figures v
Chapter One: Introduction 1
Chapter Two: Tectonic Framework of the Mount McKinley Restraining Bend 3
Chapter Three: Analog Modeling Framework and Scaling Parameters 7
3.1 Framework 7
3.2 Scaling Parameters 8
Chapter Four: Methods and Results 10
4.1 First-order uplift patterns 10
4.2 Nature of subsidiary faults 12
4.3 Migration and advection of material through the bend 13
Chapter Five: Discussion 20
5.1 First-order uplift patterns 20
5.2 Nature of subsidiary faults 22
5.3 Migration and advection of material through the bend 23
Chapter Six: Conclusions 28
Chapter Seven: Future Research 28
References 29
Vita 34

LIST OF FIGURES

Figure 2.1 Tectonic Framework 5
Figure 2.2 Mount McKinley Restraining Bend 6
Figure 3.1 Analog model 9
Figure 4.1 Modeled surfaces 16
Figure 4.2 Differenced surface 17
Figure 4.3 Nature of slip on subsidiary faults 18
Figure 4.4 Particle tracking and fault migration 19
Figure 5.1 "Teflon" Peaks 26
Figure 5.2 Eastern vertex migration. 27

CHAPTER ONE: INTRODUCTION

Although analog modeling is regularly used to simulate and examine common tectonic processes, heterogeneity of natural settings invariably results in differences between the model and the natural setting. However, recognizing that similarities exist in spite of complications in the natural setting provides the opportunity to isolate and identify first-order controls that influence the behavior of different parts of the system. We use this principle to investigate the controls on restraining bend deformation using the Mount McKinley restraining bend (MMRB) of the dextral Denali fault system in south-central Alaska as our natural setting example. Within a matter of minutes, the wet kaolin clay analog model, set up to mimic that of the MMRB, allowed us to better understand how the natural setting evolved. With each model run, it became apparent that the pattern of rock uplift and the evolution of the fault geometry in the model displayed remarkable similarity to that of our natural setting.

The Denali fault system forms a prominent arc across south-central Alaska, acting as a conduit for strain to transfer from the southern Alaska plate boundary into the continental interior. Superimposed upon the broadly arcuate fault trace, the MMRB is a large-scale left-step of the Denali fault with a through-going stepover fault segment. The stepover segment creates an ~18° bend in the Denali fault trace with asymmetrical topography and asymmetrical relief occurring along this segment. Denali (formerly Mount McKinley) is the tallest peak in North America at 6,194 m and is located within the eastern vertex of the MMRB. Despite the few thermochronologic investigations into when uplift occurred (e.g. Fitzgerald et al., 1995; Lease et al., 2016) and recent advances in Quaternary fault identification (Bemis et al., 2012; Burkett et al., 2016 (in press)), essentially no new studies have identified what the key influences and processes are that create such dramatic topography.

Advances in the understanding of the MMRB Quaternary tectonics, new and existing low-temperature thermochronometry, and new analog modeling results provide an opportunity to examine first-order controls on restraining bend evolution. In combination, these data sets allow us to address scientific questions that are integral to understanding the evolution of our natural setting. We pose three main questions: (1) Are the first-order uplift patterns independent of crustal heterogeneity and rheological contrasts? (2) What is the nature of the slip on subsidiary faults in the MMRB? (3) How did the tallest mountain in North America form within a migrating restraining bend? Using uplift patterns, localization

of deformation, formation of new faults, and displacement fields for the model set up and the natural setting, we demonstrate that first-order uplift patterns are not controlled by rock type; subsidiary faults produced in the model show oblique slip, whereas the subsidiary faults from the MMRB show pure dip-slip movement; and restraining bend geometry and slip partitioning affect how long material remains within the restraining bend and, in this case, allows for the production of asymmetric topography within a migrating restraining bend.

CHAPTER TWO: TECTONIC FRAMEWORK OF THE MOUNT MCKINLEY RESTRAINING BEND

Southern Alaska has been the focus of subduction at the Aleutian megathrust since the Mesozoic. As such, the crust consists of numerous accreted terranes, notably the Yukon-Tanana and Wrangellia terranes (Trop et al., 2002), which are bounded by major crustal boundaries and suture zones. The modern tectonic framework is strongly controlled by aspects of an ongoing subduction system that began in the Late Miocene to Pliocene (e.g. Bemis et al., 2012; Bruns, 1983; Chapman and al., 2008; Plafker and Berg, 1994). An oceanic plateau defined, as the Yakutat block (Bruns, 1983; Plafker and Berg, 1994), undergoes flat-slab subduction beneath the North American plate while a thickened section of the Pacific Plate collides into the North American Plate (Eberhart-Phillips et al., 2006) (Figure 2.1). Stresses from this collision transfer far inboard, over 600 km, and drive the rotation and active deformation throughout south-central Alaska.

An active mountain belt and a large, crustal-scale, curved fault is superimposed over the long history of terrane accretion. The boundary between the Yukon-Tanana terrane and the Wrangellia terrane is marked by the Denali fault. The Denali fault not only accommodates the collisional forces from the megathrust (e.g. Fitzgerald et al., 2014; Jadamec et al., 2013; Abers, 2008; Lahr and Plafker, 1980), but also the counterclockwise rotation of Southern Alaska (Fitzgerald et al., 2014; Haeussler, 2008). The Denali fault lies in the middle of the Alaska Range suture zone, a highly deformed terrane boundary zone (Ridgway et al. (2002) which extends from the Talkeetna thrust to the southern margin of the Yukon-Tanana terrane (Figure 2.1). Suture zones create localized, narrow, weak zones that concentrate long-term displacement (e.g. Dewey, 1977). Ridgway et al. (2002) argue that the area of the Alaska Range suture zone was reactivated around 6 Ma potentially due to a change in relative plate motion (Engebretson et al., 1985; Fitzgerald et al., 2014) and/or an increase in relative plate velocities (Engebretson et al., 1985). This timing coincides with a pulse of exhumation found in thermochronologic data from a vertical transect on Denali as well as several other studies of the Alaska Range (e.g., Plafker and Berg, 1994; Haeussler et al., 2008; Benowitz et al., 2011).

The bedrock geology within the Mount McKinley restraining bend (Figure 2.2a) consists of a series of plutons intruded into poly-metamorphosed sedimentary rocks (e.g. Reed, 1961; Reed and Nelson, 1980; Wilson et al., 1998). The crust to the north of the central Alaska Range is 26 km thick whereas beneath the central Alaska Range crustal

thickness ranges from 35-45 km (Veenstra et al., 2006). The Kahiltna Assemblage is an extensive suite of marine Jurassic-Cretaceous conglomerate beds capped with a fining upward sequence of sandstones and mudstones (Figure 2.2a) that were deposited in the closing ocean basin ahead of the collision of Wrangellia (Eastham and Ridgway, 2000). The abundant weak planes within the thinly bedded sandstones and shales accommodate diffuse deformation much more readily than the crystalline plutons. The Pliocene Nenana Gravel and potentially correlative Plio-Pleistocene deposits (brown on Figure 2.2a) are thick-bedded and poorly cemented Tertiary, Pliocene and upper Miocene alluvial and fluvial gravels that were deposited into proximal basins prior to the propagation of Quaternary thrust faults (Csejtey et al., 1992; Ridgway et al., 2007; Bemis and Wallace, 2007; Bemis et al., 2012; Burkett et al., 2016). The upper surfaces of the gravels provide flat surfaces to constrain recent uplift rates (Bemis, 2004), but act similar to the unconsolidated surficial sediments (pale yellow, Figure 2.2a) and glaciers within the MMRB to hide various contacts between units and overprint past deformation.

Most of the exhumation in the Alaska Range is constrained by thermochronologic studies (e.g. Armstrong et al., 2007; Benowitz et al., 2012; Benowitz et al., 2011; Benowitz et al., 2013; Fitzgerald et al., 1995; Fitzgerald et al., 1993; Haeussler et al., 2008; Lease et al. 2016; Nokleberg et al., 1992; Perry, 2014; Plafker et al., 1992) that indicate the central Alaska Range in the Denali area began rapid exhumation at ~6 Ma. Ridgeway et al. (2007) and Thoms (2000) illustrate late Cenozoic exhumation of the Alaska Range through foreland basin deposits, which suggests that the Alaska Range as a whole has undergone different exhumational histories and that strain accumulation is variable throughout the range due to local heterogeneities within the crust. Lease et al. (2016) determined that at ~30 Ma, the central Alaska Range underwent exhumation until ~18 Ma due to initial Yakutat contact with the North American plate. The stress from this collision concentrated along the weakened suture zone via the Denali fault. Lease et al. (2016) also conclude that successive exhumation seen in the cooling histories suggests that crust advects through the MMRB at a long-term slip rate of ~4 mm/yr within the restraining bend. Modern slip rates on the Denali fault range from ~12 mm/yr to the east of the MMRB and decrease to ~7 mm/yr west of the bend (Benowitz et al., 2011). If the 4 mm/yr slip rate estimation through the bend is correct, the 12 mm/yr slip rate is partitioned between the strike-slip Denali fault, and the active thrust faults to the north of the Denali fault.

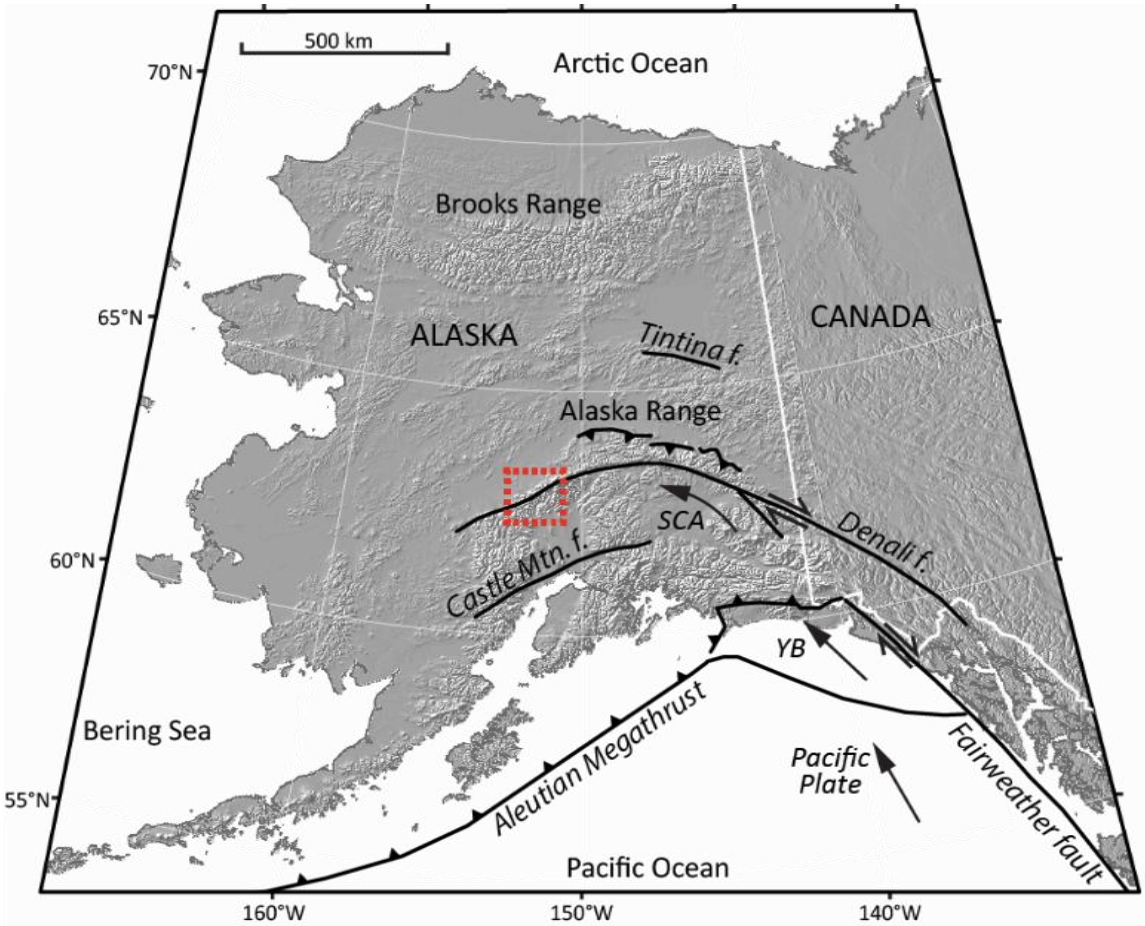

Figure 2.1 Tectonic Framework
Hillshade of Alaska with major surface fault traces. The Yakutat Block (YB) undergoes flat-slab subduction, driving the counter-clockwise rotation of southern Alaska (SCA). Stress from this collision localized along the Denali fault and created the Alaska Range. The Mount McKinley Restraining Bend is show inside the red dashed box. Black arrows are not scaled to show relative velocity. Figure modified from Bemis et al. (2012).

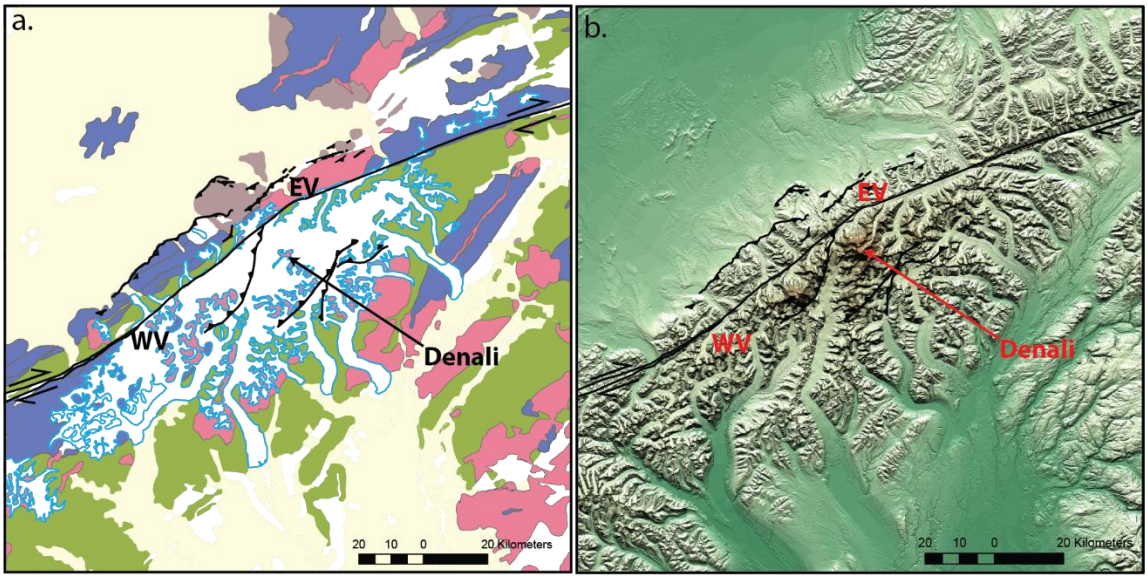

Figure 2.2 Mount McKinley Restraining Bend
EV: eastern vertex of restraining bend; WV: western vertex of restraining bend. a. Simplified geologic map of Mount McKinley restraining bend. Green = Jura-Cretaceous flysch; Brown = Plio-Pleistocene alluvial sediments (possible Nenana Gravel equivalent), Blue = Paleozoic-Mesozoic metasedimentary rocks and Tertiary undivided volcanics; Pink = Paleocene and Eocene granites; White with blue = glaciers; Yellow = unconsolidated surficial deposits. Denali fault trace and subsidiary thrust faults drawn in black lines. b. Shaded relief topography with a color elevation overlay. Higher elevations in orange and lower elevations in green

CHAPTER THREE: ANALOG MODELING FRAMEWORK AND SCALING PARAMETERS

3.1 Framework

Geometric complexities within large-scale strike-slip systems can produce localized zones of uplift (Cunningham and Mann, 2007) resulting from space problems at fault block boundaries (Crowell, 1974) and not optimally oriented fault segments that cause mechanical inefficiencies along the segments (e.g. (Hatem et al., 2015). Cunningham and Mann (2007) define bends as spatially offset areas where bounding strike-slip faults are continuously linked and continuously curved across the offset. Active bends are easily recognizable by their extreme topographic relief as well as exposed fault-bounded deep crustal rocks (Cunningham, 1995; Cunningham and Mann, 2007; Karig, 1979; Mann, 2007; Roeske et al., 2003). The through-going stepover segment of the MMRB lies between an ~18° eastern vertex and a ~13° western vertex, approximately 65 km apart (Figure 2.2a & 2.2b). Extreme topography exists adjacent to the Denali fault within the MMRB, making this feature easily recognizable. Much of the exhumation and relief within the MMRB is concentrated on the southern side of the Denali fault trace, with a less extreme and narrower zone on the northern side (Figure 2.2a & 2.2b).

The evolution of the restraining bend spans across kilometers and millions of years, but within a few minutes, simple small-scale models can replicate similar processes. Various other studies, such as McClay and Bonora (2001), Cooke et al. (2013), and Hatem et al. (2015), also connect restraining bend geometry with topographic patterns and deformation using similar sandbox set-ups but with various materials to account for scaling and material properties necessary to answer the specific questions posed by each author. McClay and Bonora (2001) published the first example of a restraining bend analog model using a sandbox experimental set up. They document the shapes and evolution of structures and faults created as the two basal plates slide through a preexisting bend in the fault (McClay and Bonora, 2001). Mitra and Paul (2011) found that initial fault geometry controls the uplift patterns near the restraining bend and that gentle restraining bends produce a more elongate region of uplift compared to the more rectangular regions from sharp restraining bends. Cooke et al. (2013) used wet kaolin experiments to examine the evolution of restraining bends with varying stepover distances and bend angles, finding that restraining bend systems evolve towards a more mechanically efficient system by propagating new faults (Cooke et al., 2013).

3.2 Scaling Parameters

The claybox used in this study is 50 cm by 20 cm with motors attached to each plate to drive the movement; however, for our analysis one plate is held fixed (Figure 3.1). A metal plate underlying the clay with a 15° angle and a 4 cm stepover distance provided the geometric set up for this model. To ensure this scaled geometry fit within the claybox, we use a scaling ratio of 1 cm clay to 3.5 km of crust. A 2.5 cm-thick layer of clay was poured on top of the metal plates and an electrified probe pre-cut a vertical, through-going fault into the clay. Cooke and van der Elst (2012) determine a wet kaolin Maxwell relaxation time $\left(\frac{2\eta}{G}\right)$ of 16 minutes. . Using an average upper crustal viscosity of 10^{24} Pa-sec and shear modulus of ~30 x 10^{9} Pa results in a Maxwell relaxation time of 2.1 My for the crust in the natural setting. We used a bi-viscous clay with a shear strength of 101.98 Pa and a water content of 71.69% by weight. As a Burger's material, the clay deforms visco-elastically with both a Kelvin and Maxwell component (thus the "bi-viscous" clay). When the clay is loaded, there is an immediate recoverable elastic response and a non-recoverable viscous response. The Maxwell component is the initial elastic and non-recoverable viscous response in series, and the Kelvin component is the recoverable time-dependent response (Cooke and van der Elst (2012). Considering the recognized westward decrease in slip rate along the Denali fault (e.g., Matmon et al., 2006; Meriaux et al., 2009), we estimated a slip rate for the Denali fault within the restraining bend of 6.5 mm/yr, or 2.5 cm/min on the analog model.

We used particle tracking velocimetry to track ~1 mm black glitter for the duration of the experiment. Tracer image resolution is at 130 pixels/cm. To correctly scale our analog model, we used both the fault geometry and thickness of the brittle crust of the MMRB as constraints for the clay box. To scale both geometry and rheological properties, the clay thickness becomes prohibitively thick for the current motors and model rigging.

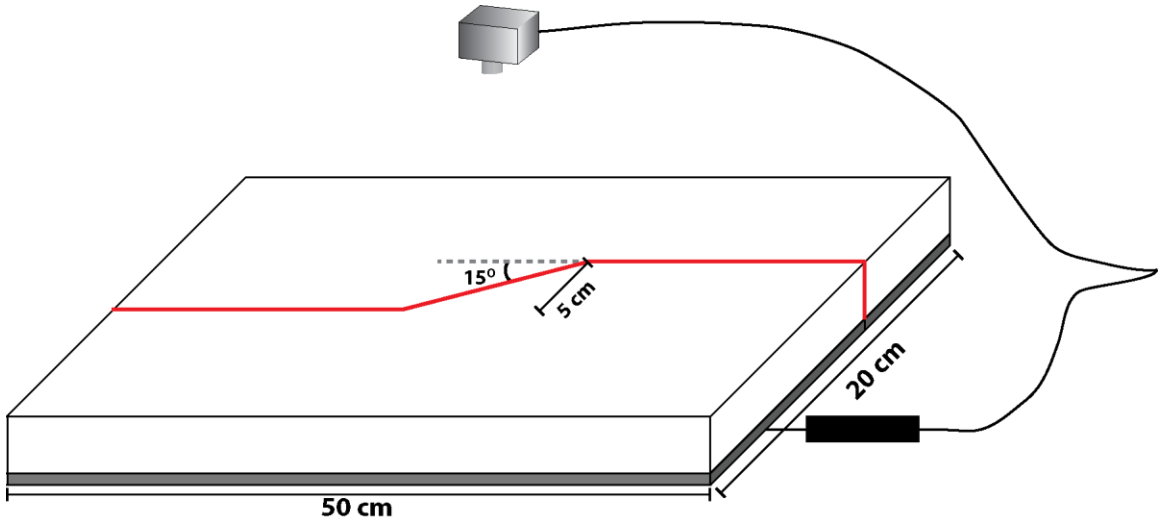

Figure 3.1 Analog model
Simplified diagram of the wet kaolin analog model set-up. Red line represents the vertical fault cut through the clay with a 15° angle and a 5 cm stepover distance. Overhead camera documents the progression of deformation during the experiment. Each underlying plate (gray) is connected to a motor (black rectangle). Topography forms on moving plate and the other plate remains fixed.

CHAPTER FOUR: METHODS AND RESULTS

Our three proposed questions guided us to answers and clarifications previously overlooked and/or assumed controls on restraining bend deformation in the MMRB. Having the ability to view long-term geologic processes in a matter of minutes provided the opportunity to test these controls. The following three sections correspond with our original questions: (1) Are the first-order uplift patterns independent of crustal heterogeneity and rheological contrasts? (2) What is the nature of the slip on subsidiary faults in the MMRB? (3) How did the tallest mountain in North America form within a migrating restraining bend?

4.1 First-order uplift patterns

The topography of the Alaska Range is characteristically asymmetric across the Denali fault with the most extreme asymmetry of orogenically created topography and relief lying within the MMRB (Figure 2.2b). To produce a quantitative comparison between the MMRB and the results from our analog modeling, we created three different surfaces in ESRI's ArcGIS (Figure 4.1). To properly classify the surfaces we created, we utilize an England and Molnar (1990) ideology. England and Molnar (1990) differentiate between three types of uplift: surface uplift, rock uplift, and exhumation. Each represents movement of rock with respect to a different frame of reference and are related via a simple equation, surface uplift = rock uplift – exhumation. Surface uplift is the displacement of the surface with respect to the geoid; rock uplift is the displacement of rock with respect to the geoid; and exhumation is the displacement of rock relative to the surface (England and Molnar, 1990). We constructed a rock uplift surface based on the rock uplift contours interpolated from apatite fission track cooling ages from Fitzgerald et al. (1995) (Figure 4.1.2a-c). A minimum estimation of rock uplift can be represented by modern topography if we assume that rocks form at some elevation (i.e. a geoid, mean surface elevation, mean sea level, etc.) and some process moved them to a different, higher elevation. This difference in position estimates the amount of rock uplift, although it ignores the effect of erosion, isostacy, and numerous other processes. For our purposes, this simplification is sufficient for estimating a *minimum* surface. Recognizing that the modern glacial valleys represent zones of erosion, we created our simplified minimum rock uplift surface by manually selecting elevation points at modern, prominent peaks and ridgecrests, as well as along the Denali fault trace. We assigned a triangulated irregular network (TIN) interpolation to construct this surface from the selected points (Figure 4.1.2a-c). To create a comparable surface for the analog

model, we follow a similar method as with the minimum rock uplift surface. However, rather than manually selecting elevation points, elevation measurements were calculated from a laser scan of the analog model after a completed run. These values represent both surface uplift and rock uplift because there is no erosion in the analog model set up, and therefore, rock uplift is equal to surface uplift. We scale the analog model surface to that of the minimum rock uplift surface by converting the elevation values from the laser scan, measured in millimeters, to kilometers (1 cm in clay = 3.5 km in natural setting) and we aligned the modeled fault trace to the modern Denali fault trace (Figure 4.1.3a-c).

By understanding the significance of what process each interpolated surface represents, we are able to understand why differences occur. The Fitzgerald (1995) rock uplift surface is noticeably (~3 km) higher than both the minimum uplift surface and the analog surface. The Fitzgerald (1995) surface represents a rock uplift surface where movement of rock is measured with respect to a geoid (in this case, the surface of the earth). Fission track cooling ages constrain rock uplift by providing an estimation of exhumation (rock uplift minus erosion). Total exhumation for Denali is ~6 km, resulting from ~9 km of rock uplift and ~3 km of erosion. Rock uplift was measured from ~3 km depth, constrained by an exposed partial annealing zone, to the present elevation of Denali (Fitzgerald, 1995). Both the minimum uplift surface and the analog surface represent surface uplift, or movement of rock with respect to the surface of the earth. However, in this scenario, rock uplift and surface uplift are equivalent, as we have no erosion in either surface. The lack of a second (western) vertex in the Fitzgerald (1995) surface creates a discrepancy between it and the other two interpolated surfaces. The lack of this geometry control results in a surface without an elongate, fault-parallel deformation zone (Figure 4.1). Another difference between the surfaces results from material advecting through the bend. Bemis et al. (2016) include advection of material through the bend into their analysis of the MMRB and our analog model exhibits advection of material through the bend. Fitzgerald's (1995) surface only includes vertical movement of rock, not advection through. This advection creates a gentle sloping uplifted volume of rock while the steep, plateau-like Fitzgerald (1995) surface results from no advection.

The minimum rock uplift surface and the experimental surface generally show very similar exhumation patterns (Figure 4.1). A narrow zone (<20 km) of deformation is present on the north side of the Denali fault trace, whereas a larger, wider zone (30-40 km) exists on the southern side of the fault. The zone of deformation on the southern side of the

Denali fault in both the minimum rock uplift surface and the clay surface reaches approximately the same distance from the fault trace (note the modern, southern thrust faults printed on each surface, Figure 4). Remarkably, the clay surface shows two peaks in the broad zone of deformation that spatially correspond to the peak of Denali to the east and Mount Foraker to the west. Because the topography-derived surface excludes erosion, we do not expect the shapes of the peaks to match between the surfaces; however, the spatial alignment of these high zones suggests a common causal mechanism during the evolution of these bends.

Although the model produced similar spatial patterns to the natural setting, it did not manage to produce an equivalent amount of surface uplift. The highest point on the clay surface, ~1.3 cm above the starting elevation, scales to ~4.5 km, whereas Denali itself is ~6 km high (Figure 4.1). To better understand this discrepancy, we aligned the clay model surface and the minimum rock uplift surface of the MMRB subtracted them from each other to produce a visual comparison of the surfaces (Figure 4.2). Although both surfaces show generally the same pattern of deformation (asymmetric topography and a broad zone of deformation to the south of the fault trace and a narrow zone on the north), the analog surface clearly did not produce enough topography to mimic that of Denali.

4.2 Nature of subsidiary faults

We used the displacement and shearing of the reference grid imposed on the surface of the experiment to test if lateral motion across the subsidiary faults within the experiment is consistent with similarly positioned faults in the MMRB. After the full duration of the experiment, gridlines were both laterally offset across the faults, as well as exhibiting simple shear adjacent to the fault trace. Bemis et al. (2012) saw no lateral offset on the northern thrusts in the MMRB, indicating a pure dip slip movement in the present-day. Figure 4.3 shows the sheared lines in the clay near the fault and displaced but linear lines farther from the fault, as well as a series of features (valleys, glacial moraines, and fault-parallel fissures) of the MMRB with no lateral offset. Particle tracking velocimetry also revealed lateral movement along the northern thrust faults. Most apparent, the central-cluster particle closest to the main cut of the fault moves due west and then bends to the northwest (Figure 4.4). Despite this very apparent difference between the analog model and the natural setting, the observations by Bemis et al. (2012) are only constrained by late Quaternary landforms. Particle paths illustrate a temporal change in the ratio of fault normal vs fault parallel slip as shown by the curvature of the particle trajectories (Figure

4.4). Our model shows the development of the restraining bend while the natural setting is the result of a more complex history than our modeling environment. Therefore, movement on the thrust faults in the MMRB could have initiated similarly, with oblique movement, but as the system evolved and the Denali fault became more mature, slip became partitioned.

4.3 Migration and advection of material through the bend

Burkett et al. (2016 (in press)), present a simple model based on geologic evidence where the eastern vertex of the MMRB is migrating to the southwest. To test this proposed model, we used particle tracking velocimetry (PTV) to examine whether or not the restraining bend migrates in our analog model and how material advects through the bend. Burkett et al. (2016 (in press)) hold the north side of the Denali fault fixed for their model, and we wanted to ensure we had a similar reference frame when comparing their model to our analog model PTV results. We selected clusters that consist of representative points that show the particle trajectories across target regions of the model (i.e. bend vertices) (Figure 4.4). By tracing and following representative but individual particle paths at various spatial locations on the model, we notice three distinct patterns: (1) particle migration rate decreases as distance increases from the fault on the stationary (northern) plate; (2) paths change in direction as the particle passes through the bisector of the bends (3) as the main subsidiary thrust fault initiates, particle rate decreases near where the fault propagates (western vertex) (Figure 4.4).

Central particle cluster

Particles c_1-c_5 (Figure 4.4) were selected to highlight the decrease in displacement with distance from the fault trace, as well as an overall deceleration. All particles to the north of the fault trace initially migrate west, but finish with a northwest trajectory C_1 and nearby particles hardly migrate, as indicated by the short particle path (Figure 4.4), suggesting that the clay even farther north remains fixed throughout the duration of the model run. We expect a fixed point in the model, as one plate does not move during the model. The first time slice (t_0-t_1) the main fault trace stepover segment migrates to the west and maintains a sub-parallel geometry to the original cut fault. As the most prominent/largest subsidiary thrust fault forms at the western apex of the main strike-slip fault, the particles decelerate form north to south, as well as east to west (Figure 4.4).

Eastern particle cluster

Particles e_1-e_4 (Figure 4.4) follow a southwest trajectory for the duration of the model run. The total displacement (line length, excluding direction) per time elapsed for

each path has consistent trends between all paths. The southernmost particle (e_4, Figure 4.4) traveled the longest distance, because of its location relative to the structurally complex vertex of the bend. As predicted by the Burkett et al. (2016 (in press)) particle migration, when a particle passes through the bisector of the vertex angle, the path will bend. The second particle down from the main fault (e_2, Figure 4.4) trace demonstrates this concept; in the t_1-t_2 time slice (green on Figure 4.4) there is a clear bend in the particle path at the vertex bisector. Although the other particles do not all show such a dramatic kink, the paths do all curve and have generally the same total displacement. Our model differs from the Burkett et al. (2016 (in press)) because our analog model is a continuous system with no discrete time "steps".

Western particle cluster

The particle paths (w_1-w_5, Figure 4.4) trend to the west overall and displacement increases from north to south. However, given each path's position to the main thrust fault, the individual paths do differ from one another. From north to south, the overall particle paths become more east/west than northeast/southwest. The southernmost particle, w_5, and nearby particles are outside of the thrust by the time of initiation, and therefore, continue in a straight path. All paths converge at an angle parallel to the main fault trace outside of the stepover segment. The second particle down from the north (w_2, Figure 4.4) has a particle path most different from the others. The first three intervals, t_0-t_1, t_1-t_2, and t_2-t_3, (green, purple, and pink in Figure 4.4) and the final two intervals, t_4-t_5 and t_5-t_6 (red and yellow in Figure 4.4) have similar trajectories and overall length, but the t_3-t_4 interval (light blue in Figure 4.4) is significantly shorter. At this interval, the main thrust fault has reached its full length. Particle w_2 (Figure 4.4) remains at the junction of the main thrust fault and the strike-slip fault fromt_2 until the end of the model and has the shortest particle path of all the w-cluster particles.

Fault trace and bend vertices

As displacement accumulates along the fault in our analog model, the stepover segment fault trace and bend vertices migrate to the west. The stepover segment remains mostly parallel to the original fault trace during migration. Burkett et al. (2016 (in press)) present a simple geometric argument for along fault migration of the MMRB using discrete time steps and a single vertex to distill the complex bend down to its most simple vectors. We use a similar set up to understand the controls on our analog model but are working with a continually moving system with two vertices and the initiation of a main thrust fault.

In the Burkett et al. (2016 (in press)) model, a single vertex (similar to our eastern vertex) migrates to the southwest and the stepover segment migrates to the northwest, while remaining parallel to the original trace. Our analog model is more similar to the natural setting than the Burkett et al. (2016 (in press)) model. It initiates with sharp, 15° eastern and western vertices and a straight, through-going stepover segment. With more displacement, the sharp vertex angles become more rounded and migrate to the west along with the stepover segment. The stepover segment becomes less linear and the migration rate decreases once the main thrust fault initiates. In the final three time steps, t_3-t_4, t_4-t_5, and t_5-t_6 (light blue, red, and yellow on Figure 4.4) the eastern vertex and stepover segment remain fairly fixed, but the western vertex continues to migrate further west, elongating the stepover segment. The eastern vertex and stepover segment appear to migrate together throughout the model, but because the main thrust fault accommodates lateral slip and/or because of the increasing curvature of the bend vertex, the western vertex does not have the same rate of migration. Although different parts of the system are migrating at various rates in the model and the natural setting, the end result of an elongating stepover segment is consistent.

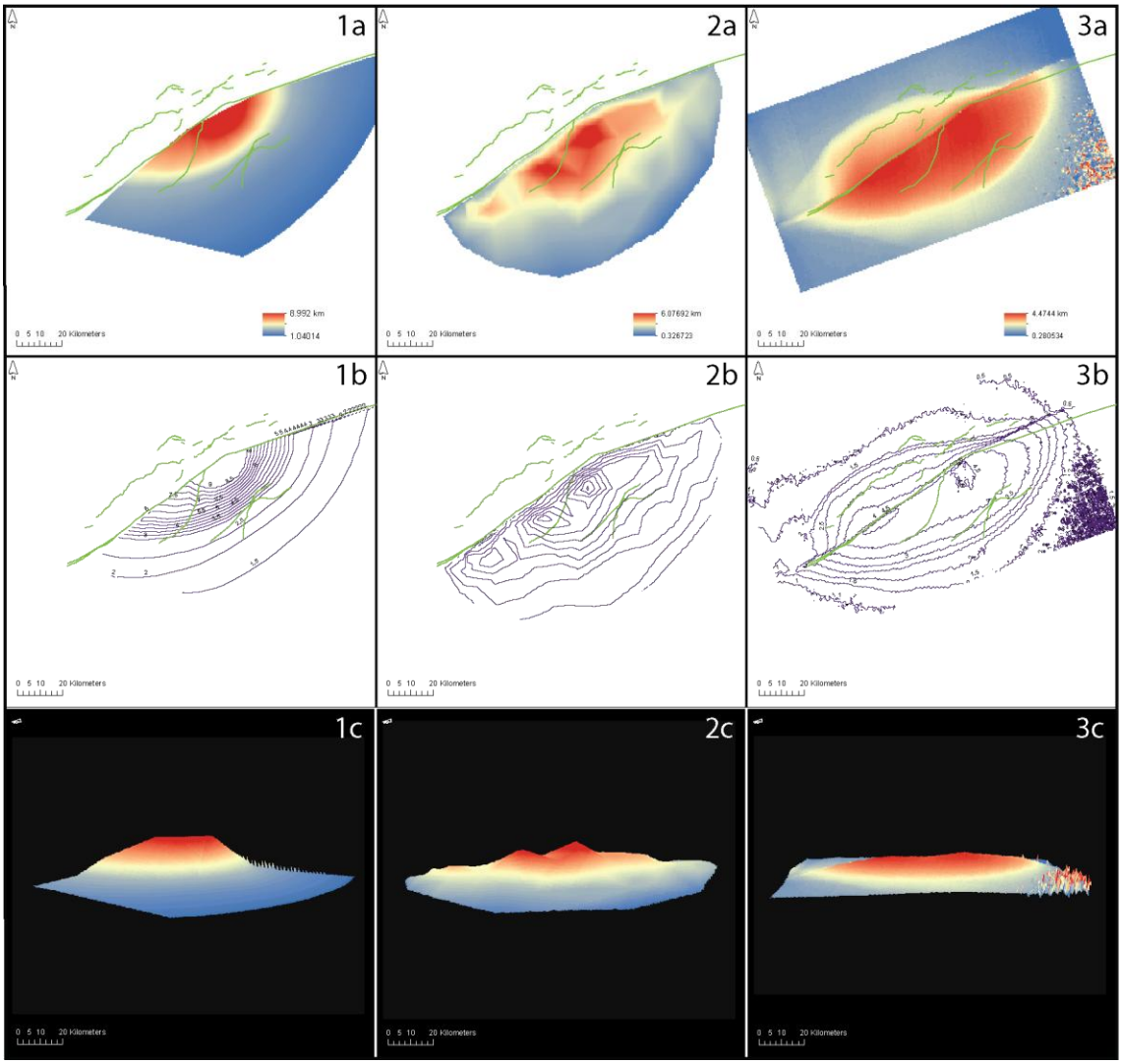

Figure 4.1 Modeled surfaces
Surfaces representing different constraints on uplift from the MMRB (1 &2) and from our wet kaolin analog model (3). 1 = rock uplift derived from the Fitzgerald (1995) surface; 2 = minimum rock uplift surface derived modern peak and ridge elevations in the Mount McKinley restraining bend; 3 = the equivalent of rock uplift displayed by the clay analog model surface. All the top images (labeled with an a) show a bird's eye view of the surfaces with modern fault overlay (green lines). The middle images (labeled with a b) show contour maps of the surfaces created in the a boxes. Contour interval = 0.5 km. All lower images (labeled with c) show an oblique view of the surfaces. Color scales from a images are the same in the c images. The southwest corner of the clay surface (image 3) is noise resulting from the laser scan. Yellow star in 3a and 3c indicate area of transition from active thrust west of the star and active normal faults east of the star (Burkett et al. (2016 (in press)).

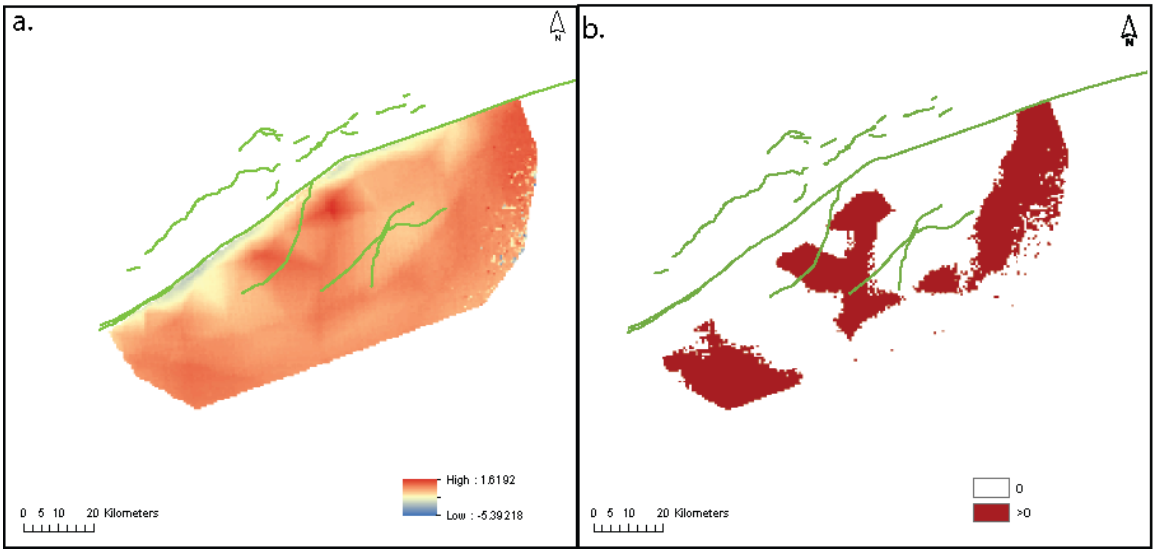

Figure 4.2 Differenced surface
Difference surface created from subtracting clay analog model surface elevations from minimum rock uplift surface elevations. Green lines represent surface traces of modern faults. A shows the unedited result of differencing the surfaces from one another. B highlights the areas that are greater than 0 after differencing the surfaces. Note: area to the east and west may result from sample noise, but central area highlights the two peaks (Denali and Mt. Foraker) where the modeled surface is not able to produce adequate topography.

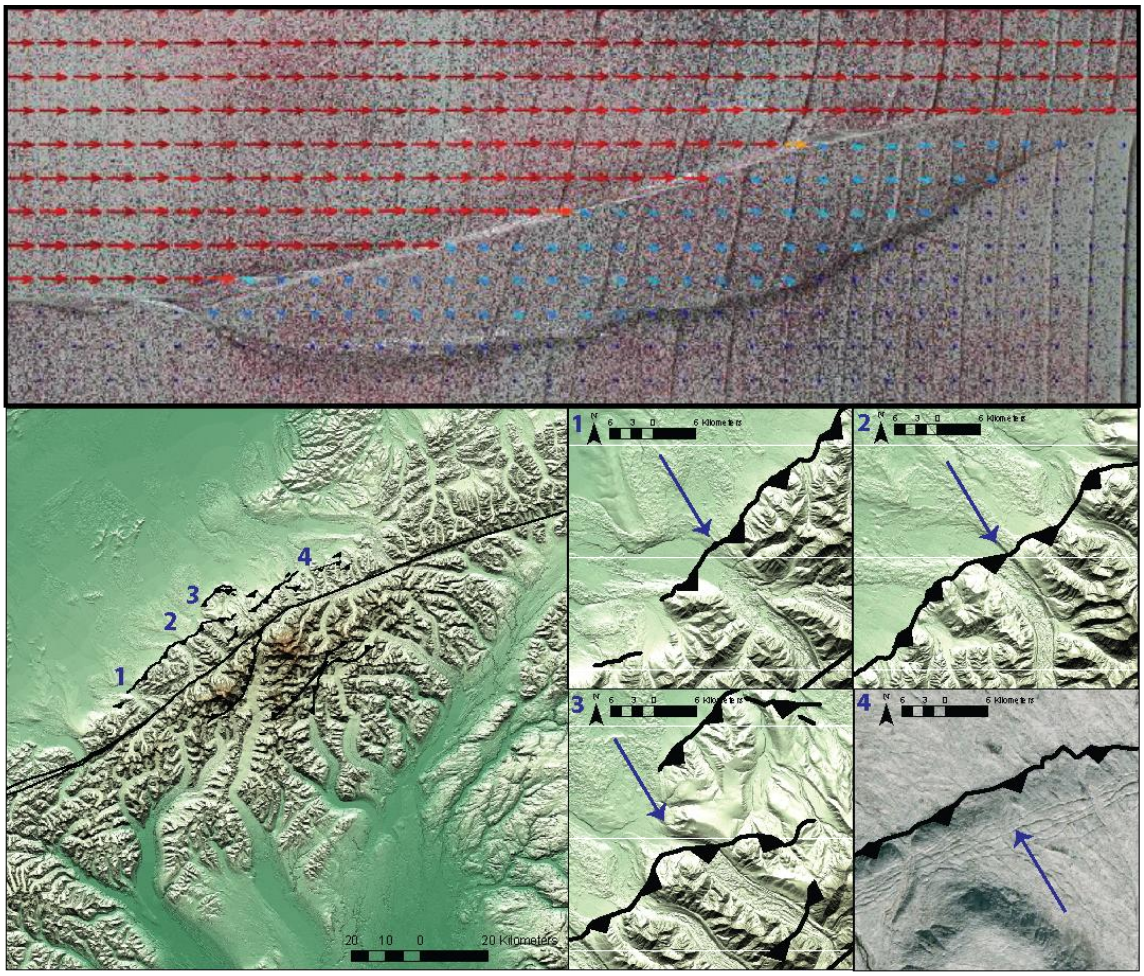

Figure 4.3 Nature of slip on subsidiary faults
Subsidiary thrust faults of model and Mount McKinley restraining bend. Top image Shows final image of an analog model run. Grid lines started straight and have been offset through the model run. MMRB images are digital elevation models while the bottom right image is from Google Earth. Inset numbers correspond to locations on main MMRB DEM. Note no lateral offset of glacial moraines or valleys. Image 4 shows a ~15 m scarp and fault parallel fissures with no offset. Scarp results from multiple earthquakes.

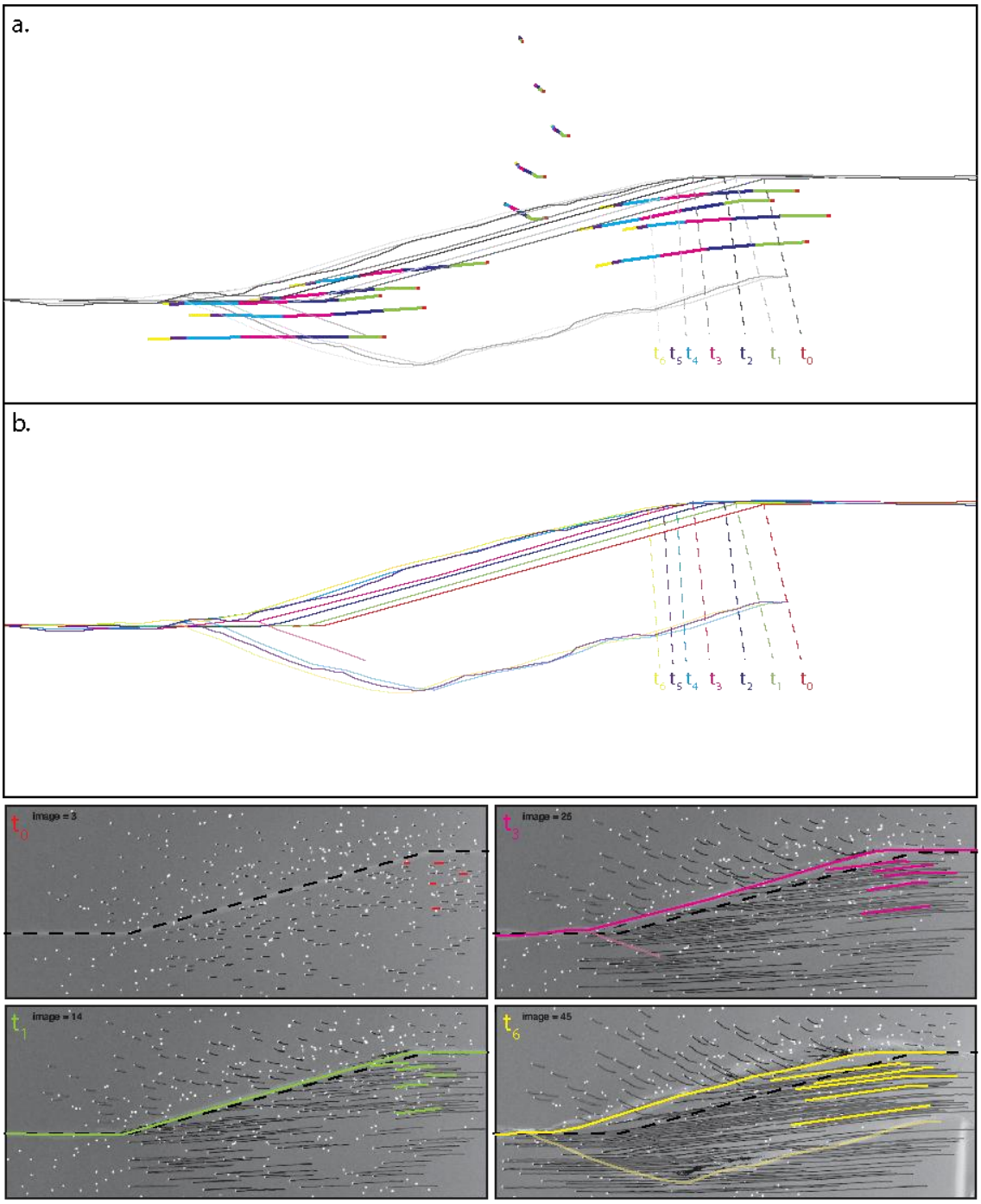

Figure 4.4 Particle tracking and fault migration
Simplified schematic showing particle migration (a.) and fault migration (b.) through duration of model at different time intervals. Lower images show four time intervals, corresponding to time intervals in a. and b, overlaid on an image resulting from PTV analysis. By selecting a few, representative points to track, the key features of the tracks are more easily recognized.

CHAPTER FIVE: DISCUSSION

5.1 First-order uplift patterns

The first-order uplift pattern similarities between wet kaolin analog models (Cooke reference) and the MMRB were the primary motivation for this study. Our new analog model scaled to the MMRB continues to reproduce the characteristic topographic asymmetry across the primary strike-slip fault. This asymmetry is defined by topography and active thrust faults occurring closer to the fault trace on the north side of the restraining bend. The extent of uplift on either side of the fault in the model is also consistent with the MMRB. Furthermore, there are distinct similarities between the model and the MMRB in the faulting/uplift patterns across the vertices of the restraining bend. For example, Burkett et al. (2016 (in press)) document a rapid transition in the style of faulting north of the Denali fault across the eastern vertex of the MMRB. This transition from active thrust faults west of the vertex to active normal faults east of the vertex occurs over a distance of less than 2 km and the region of active normal faulting corresponds with a region of effectively no uplift in the model (Figure 3.1a and 3.1b)

Examination of smaller-scale features and quantitative comparisons of uplift estimates illustrate that this model does not reproduce all the key characteristics of the MMRB. In particular, the model produces a maximum elevation of only ~4.5 km (~1.3 cm unscaled), which is ~1.5 km less than the peak elevation of Denali (Figure callout?) and ~4.5 km less than the total rock uplift derived from low-T thermochronology (Fitzgerald et al., 1995). Possible contributions to this discrepancy include, 1) different initial topographic conditions between the model and MMRB, 2) lack of erosionally-induced relief production in the model, and/or 3) the ability of local structures and crustal heterogeneity to drive additional uplift.

Different initial topographic conditions between the model, which begins with a horizontal, planar surface, and the pre-Denali (pre-6 Ma) MMRB region are certain. Tectonically-driven uplift was underway in the MMRB prior to 6 Ma (e.g. Fitzgerald et al., 2014; Lease et al., 2016; Terhune et al., 2015) and, even if occurring at relatively slow rates, this could maintain sufficient pre-existing topography to explain the 1.5 km difference between the model surface height and the peak elevation of Denali. However, in terms of rock uplift, the ~4.5 km difference between post ~6 Ma rock uplift (Fitzgerald et al., 1995) and the equivalent uplift from the model is independent of pre-existing topography.

The influence of glacial erosion is a fundamental difference between the analog model setup and the MMRB. Glaciers produce localized zones of erosion, resulting in enhanced relief production, isostatically-driven uplift, and possible increase in tectonically-driven uplift (Brocklehurst and Whipple, 2007; Brozović et al., 1997; Small and Anderson, 1995; Thomson et al., 2010; Whipple et al., 1999). With no erosion or isostatic compensation occurring in our analog model, can the ~4.5 km discrepancy in rock uplift be explained through these glacial erosion-related processes? We used a simple calculation using the ratio of the density of the crust (2.7 g/cm$^{3)}$ to density of the mantle (3.3 g/cm^3) multiplied by the amount of erosion to estimate the isostatic compensation after erosion. The equation is consistent with Burbank and Anderson (2011) who associate roughly $^5/_6$ of mean erosion to isostatic compensation. Using the exhumation estimates of Fitzgerald et al. (1995), ~3 km of crust was removed from the top of Denali, which would only result in ~0.5 km of net elevation loss.

Heterogeneity in the crust of the MMRB produces planes/zones of weakness that have accommodated the development of major faults at intermediate positions other than the single, outboard fault produced in the model. The Quaternary faults superimposed on the analog model surface clearly do not align with any particular feature produced in the model (Figure 2.2b). Although heavily glaciated, the thrust faults south of the primary strike-slip fault correspond with the contacts between granitic plutons (pink) and flysch (green) (Figure 2.2a). The lack of heterogeneity and of intermediate thrust faults in the analog model suggest that the smaller scale irregularities are not independent of crustal heterogeneity.

Ward et al. (2012) propose a "Teflon Peaks" hypothesis in which glaciation and erosionally resistant granitic peaks (like Denali) provide a positive feedback mechanism for the creation of topographic relief (Figure 5.1). Essentially, the granitic peak is too steep and smooth to form new glaciers because little to no ice or snow can accumulate. Instead, the snow and ice collects onto the valley glaciers, providing material to sustain them. At altitudes greater than 5 km, the glaciers that do exist remain frozen and cause no erosion. Isostatic rebound and tectonic rock uplift are driven from the continued incision of the valley glaciers. Compared to flexural wavelength of the lithosphere, plutons are small and therefore, when mass is removed, they are raised further. In combination, the erosionally induced relief and the local heterogeneities in rock type drive localized uplift. Therefore, the ~1.5 km difference between the true Denali peak elevation of the MMRB and the "Denali"

from the analog model may result from smaller scale forcings that our model is unable to replicate.

5.2 Nature of subsidiary faults

The nature of slip on the faults within a strike-slip system provides clues into the degree of slip-partitioning, structural connectivity, and the maturity of the primary fault zone (e.g. Stirling et al., 1996; Wesnousaky, S.G., 1988). Bemis et al. (2015) argue for a high-degree of slip-partitioning across the Denali fault system throughout the Alaska Range based on the systematic pattern of Quaternary faults recording shortening orthogonal to the Denali fault, while the Denali fault remains primarily strike-slip. Quaternary fault mapping from Bemis et al. (2012) and Burkett et al. (2016 (in press)) in the MMRB document dominantly dip-slip motion on thrust faults north of the Denali fault and Haeussler (pers. Comm. 2015) notes dip-slip motion on the thrust faults to the south (Figure 2.2a and 2.2b). Although direct slip markers are unknown for the MMRB portion of the Denali fault, the contrast in elevation and rock uplift across the fault suggests a component of vertical slip on the stepover segment of the Denali fault. However, with <6 km of relative rock uplift since 6 Ma, the vertical slip rate across the Denali fault would be <1/6th the lateral slip rate. Therefore, despite the inferred oblique slip on the Denali fault within the MMRB, the dip-slip motion on the subsidiary thrust faults suggests a high degree of slip-partitioning that is consistent with the rest of the Denali fault system within the Alaska Range.

The particle trajectories in the wet-kaolin model suggest that the degree of slip partitioning evolves through the course of the experimental run. Initially, the particles north of the stepover segment move parallel to the stepover segment before curving towards the northwest and ending with a trajectory near perpendicular to the Denali fault (Figure 4.4). The transition from parallel to perpendicular displacement suggests an increase in slip partitioning between the primary strike-slip fault and the subsidiary faults. We interpret this behavior to be analogous to increasing fault maturity, such that with increased slip across the primary strike-slip fault it develops a continuous, well-connected fault zone structure that more readily accommodates displacement parallel to the fault plane. The wet kaolin model probably develops fault maturity through the organization of the fault planes to minimize work (e.g., Michele's Work/restraining bend paper), and the rotation of clay particles to be parallel with the fault, enhancing the weakness of the fault zone from the preferred orientation of planar particles.

Dolan and Haravitch (2014) found that surface slip on structurally mature faults with large-cumulative-displacement (>85 km) are similar to slip measurements at depth, suggesting mature faults have fewer and smaller zones of structural complexities and a smaller component of off-fault deformation. They suggest a mature fault with a typical "smoothness" to its surface trace is capable of accommodating 85-95% of slip on the main fault trace. If the Denali fault is a mature fault, it would be able to accommodate most of the slip parallel to its fault plane, leaving only an orthogonal component of slip to be accommodated. With a high degree of slip partitioning (Bemis et al., 2015) and substantial (300-400 km) cumulative slip east of the MMRB and at least 140 km of post-Cretaceous slip west of the MMRB (Miller et al. 2002; Blodgett and Clough, 1985), as well as a localized, single, through-going structure, we infer that the Denali fault is presently a mature fault through the MMRB.

The production of oblique slip on the subsidiary faults in the analog model suggests an intrinsic difference between the model and the MMRB. The relative amount of lateral slip across the subsidiary fault trace changes long the length of the fault. Where the subsidiary fault is more oblique to plate motion, lateral slip is higher (Figure 4.3). In terms of recent activity, the thrust faults south of the MMRB (Figure 2) are the least constrained faults in the system. The thrust faults north of the restraining bend have a relatively small component of lateral slip compared with the shortening component. Although wet kaolin clay allowed us to properly model the geometry of the MMRB, it may prohibit the system from reaching as high a degree of slip partitioning as observed in the MMRB and/or the model does not run for a long enough time to reach the level of maturity expressed by the MMRB.

5.3 Migration and advection of material through the bend

Although along fault migration of restraining bends (relative to previously deformed deposits) has received limited attention, Wakabayashi (2007) presents simple models of potential mechanisms that accommodate migration based on his documentation of migrating restraining bends in the San Andreas fault system. These models describe restraining bend migration as occurring through the creation of new stepover segments and abandonment of the previous stepover, causing the position of the bend to progressively migrate with each new cut of a stepover segment (Wakabayashi, 2007). The models allow general predictions about cumulative deformation within a migrating restraining bend,

such as limited topographic growth or rock uplift and the lack of a continuous, through-going fault.

The evidence for along-fault migration of the eastern vertex of the MMRB by Burkett et al. (2016 (in press)) is consistent with our observations of migration of the primary fault trace within the wet-kaolin analog model (Figure 4.4). In general, this migration is accommodated by the northwestward translation of the stepover fault segment accompanied by a rolling-hinge-like migration of the eastern and western vertices. To compare the migration rates for the Burkett et al. (2016 (in press)) model to those from our analog model, we tracked the displacement of the vertices through the experimental run and calculated rates based on the elapsed time of the experiment. To allow a direct comparison, these rates are converted to mm/yr using the scaling properties of the model. The stepover segment translated ~1.4 cm (orthogonal to stepover segment) in 48 min, resulting in a shortening rate of 0.8 ± 0.1 mm/yr across the narrow deforming zone north of the stepover segment. The vertex migration rates in the model are complicated by a rate change corresponding with the development of the major subsidiary thrust fault on the south side of the restraining bend and an increasing uncertainty in vertex location due to progressive rounding of the vertices (Figure 5.2). We constrain this vertex location uncertainty by also measuring displacements for maximum and minimum vertex positions for 14 stages of the model and find the resulting rate uncertainty stabilizes at ± 0.2 mm/yr after the initiation of the subsidiary thrust fault. Prior to initiation of the subsidiary thrust fault, the eastern vertex migrates at 3.6 mm/yr with negligible uncertainty in the vertex location, and after thrust fault initiation, the eastern vertex slows to 2.8 ± 0.2 mm/yr. Although partially derived from tentative age correlations of offset landforms, the stepover translation rate (1-1.5 mm/yr) and vertex migration rate (2-6 mm/yr) predicted by Burkett et al. (2016 (in press)) are consistent with these values extracted from the analog model.

As initially discussed by Burkett et al. (2016 (in press)), the association of high topography/long-term rock uplift with a migrating restraining bend is in contrast to predictions from the Wakabayashi (2007) migration models. The formation of high topography through this mechanism of bend migration is unlikely because material does not advect into and reside within the bend for an extended period of time; instead, new material is incorporated by activating a new fault strand while material previously within the bend is abandoned. With a slip rate of 6.5 mm/yr entering the stepover segment of our analog model, a particle would remain within the bend for ~10 million years. Therefore

once a particle passes through the vertex and into the bend, it will undergo a greater component of contractional strain for a significant amount of time. In the natural setting, the slip rate leaving the bend is almost half that of the slip rate entering the bend. Material would remain in the bend in the natural setting for even longer than the model suggests. Burkett et al. (2016 (in press)) suggest four interrelated mechanisms to drive persistent rock uplift in the MMRB: 1) asymmetric development of topography associated with gentle restraining bends restricts the contractional component of deformation to a narrower zone, 2) a ~65 km long restraining stepover segment means that once a piece of crust moves into the bend, it will remain in the region of contraction for millions of years, 3) if the stepover fault segment persists, the focused uplift is not abandoned by the creation of new stepover segments that occurs in traditional migrating restraining bends (Wakabayashi (2007), and 4) potential fault geometries required to maintain the same fault trace through the restraining bend while simultaneously translating it, require the involvement of a dipping fault that would additionally drive rock uplift adjacent to the stepover segment. In our analog model, uplift is confined to a narrow zone; material remains in the bend for a significant amount of time; the main fault trace is visible through the entire model and remains through-going; and we expect that our main fault trace is dipping such that it enhances uplift. Because our results are consistent with those of Burkett et al. (2016 (in press)), we suspect that numerous, if not most, restraining bends in major, mature strike-slip faults migrate in a similar fashion, but the constraints are typically difficult to work out and rarely is there a clear reference frame to model or track migration from.

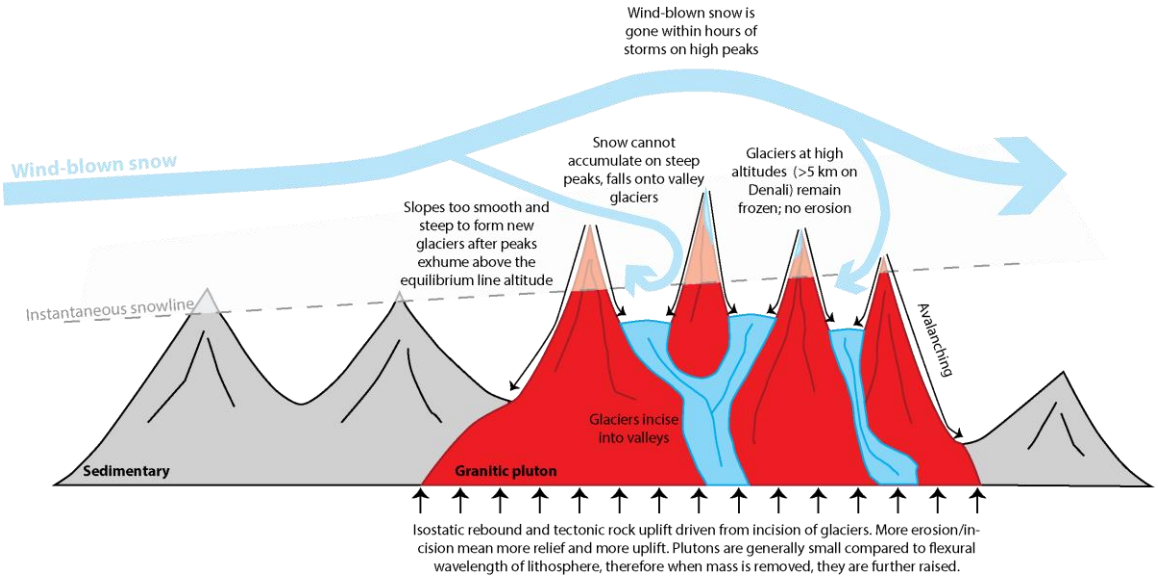

Figure 5.1 "Teflon" Peaks
Modified figure from Ward et al. (2012) depicting the "Teflon Peaks" hypothesis. The steep granitic peaks do not allow for the accumulation of snow and ice which, in turn, cannot erode the peaks. The incision of valley glaciers deeper into the pluton drives an isostatic response, increasing the elevation of the peaks. An increase in erosion or incision provides a positive feedback for relief production, driving the pluton to higher elevations.

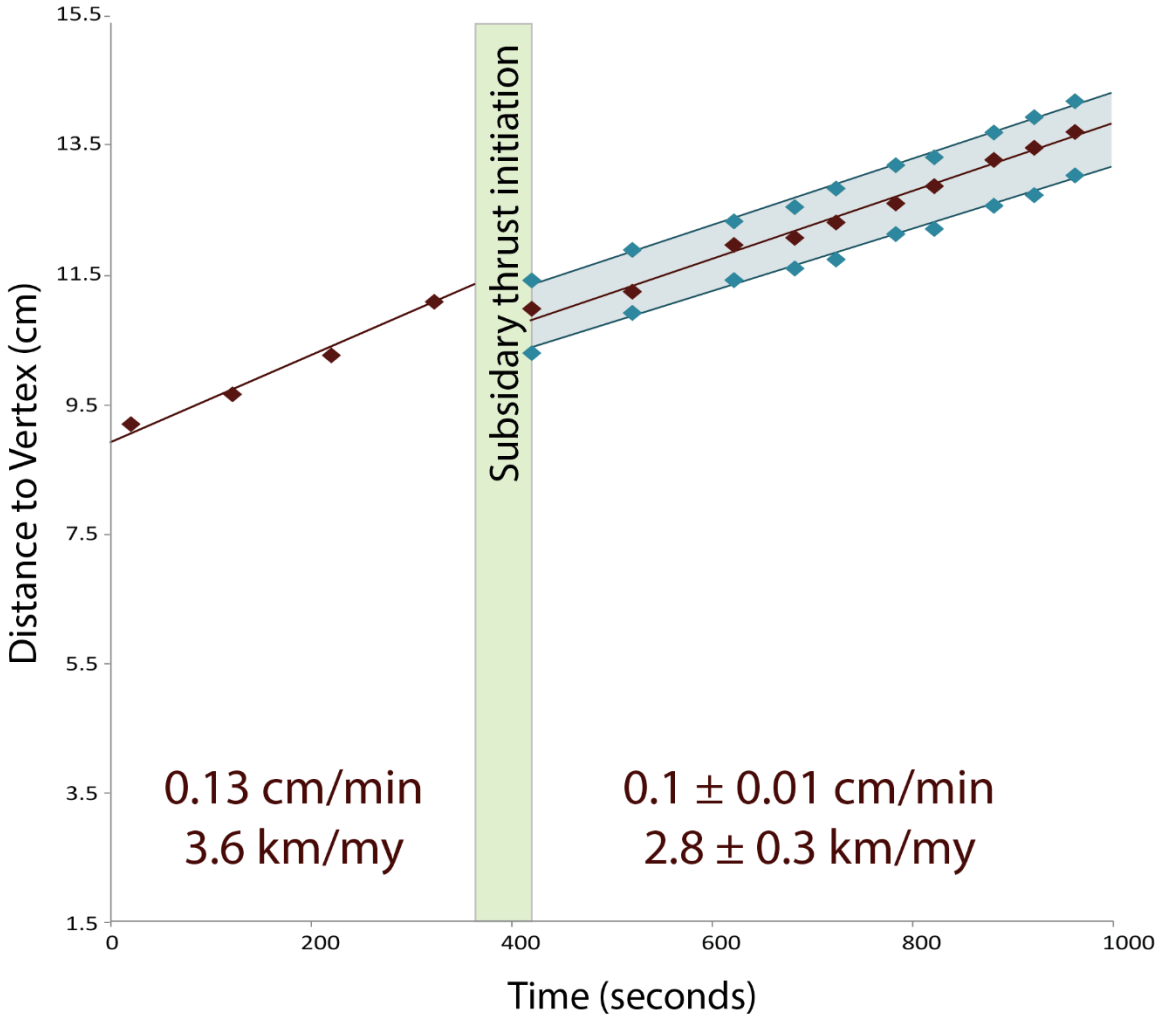

Figure 5.2 Eastern vertex migration.
Calculation of error margins for vertex angle evolution. The green diamonds represent the furthest extend of the deformed vertex. Red represents the max curvature of the bend and blue represents the point where curvature begins. We plot photo intervals as a proxy for time since the model began against the distance from the left-most margin of the image. Green and blue envelopes represent the margin of error, Note: the maximum curvature envelope (green) is consistently smaller than the minimum curvature envelope (blue).

CHAPTER SIX: CONCLUSIONS

The distribution of topography relative the trace of the Denali fault through the MMRB is remarkably similar to the results of wet kaolin analog modeling that show asymmetric development of topography across the primary strike-slip fault within the restraining bend. We have exploited this similarity by developing a wet kaolin analog model scaled to the geometric properties of the MMRB to examine the first-order controls on rock uplift/exhumation and the evolution of the fault system within this migrating restraining bend. We find that 1) first order uplift controls are independent of crustal heterogeneity, but smaller scale features, such as the peak height and rock uplift of Denali, may be enhanced by major faults exploiting rheological contrasts; 2) Although our model shows a different nature of slip on subsidiary thrust faults, the system evolves to be a more mature fault system. Perhaps our model did not run long enough to mimic the maturity of the MMRB, but it does evolve towards it; 3) previously understood models for migrating restraining bends do not adequately explain the migration of the MMRB. We support findings by Burkett et al. (2016 (in press)) that resulting extreme topography found in the MMRB is created and sustained by the geometry, slip rate, and resulting amount of time material remains in the restraining bend.

CHAPTER SEVEN: FUTURE RESEARCH

We recognized a number of shortcomings and unknowns that introduce uncertainty into our results. These issues could be addressed through additional experimental analog model runs that are set up to control for primary fault dip, as well as for both rheological properties and geometry. Recognizing the smaller-scale differences presented from the analog model, the potential role of fault dip could be tested by pre-cutting a dipping fault into the model rather than a vertical fault. Although the current modelling rig cannot accommodate it, a model run where both rheological properties and fault geometry are scaled simultaneously would also reduce uncertainty in the respective roles of model properties in controlling deformation. These results also motivate new research into mechanisms for bend migration to discern the various ways in which migration is accommodated.

REFERENCES

Abers, G. A., 2008, Orogenesis from Subducting Thick Crust and Evidence from Alaska: Active Tectonics and Seismic Potential of Alaska Geophysical Monograph Series 179 (eds J.T. Freymueller, P.J. Haussler, R.L. Wesson and G. Ekstrom).

Armstrong, P. A., Haeussler, P. J., and Arkle, J. C., 2007, Rapid Quaternary exhumation of the Eastern Alaska Range: paper 29-6 presented at Geological Society of America Abstracts with Program, Cordilleran section meting, 4-6 May.

Bemis, S.P., 2004, Neotectonic framework of the north-central Alaska Range foothills, University of Alaska Fairbanks, M.S. thesis.

Bemis, S. P., Carver, G. A., and Koehler, R. D., 2012, The Quaternary thrust system of the northern Alaska Range: Geosphere, v. 8, no. 1, p. 1-10.

Bemis, S. P., Weldon, R. J., and Carver, G. A., 2015, Slip partitioning along a continuously curved fault: Quaternary geologic controls on Denali fault system slip partitioning, growth of the Alaska Range, and the tectonics of south-central Alaska: Lithosphere, p. 12.

Benowitz, J. A., Bemis, S. P., O'Sullivan, P. B., Layer, P. W., Fitzgerald, P. G., and Perry, S. E., 2012, The Mount McKinley Restraining Bend: Denali Fault, Alaska: Geological Society of America Abstracts and Program, v. 44 (7), p. 597.

Benowitz, J. A., Layer, P. W., Armstrong, P. A., Perry, S. E., Haeussler, P. J., Fitzgerald, P. G., and Vanlaningham, S., 2011, Spatial variations in focused exhumation along a continental-scale strike-slip fault: The Denali fault of the eastern Alaska Range: Geosphere, v. 7 (2), p. 455.

Benowitz, J. A., Layer, P. W., and Vanlaningham, S., 2013, Persistent long term (c. 24 Ma) exhumation in the Eastern Alaska Range constrained by stacked thermochronology: in *Advances in 40Ar/39Ar Dating: From Archaeology to Planetary Sciences*, edited by F. Jourdan, D.F. Mark, and C. Verati, Special Publications Geological Society of London.

Blodgett, R.B., and Clough, J.G., 1985, The Nixon Fork terrane-- part of an *in situ* peninsular extension of the Paleozoic North American continent: Geological Society of America Abstract 17:342.

Brocklehurst, S.H., and Whipple, K.X., 2007, Response of glacial landscapes to spatial variations in rock uplift rate: Journal of Geophysical Research, v. 112, no. F2.

Brozović, N., Burbank, D.W., and Meigs, A.J., 1997, Climatic Limits on Landscape Development in the Northwest Himalaya: Science, v. 276, no. 5312, p. 571-574.

Bruns, T. R., 1983, Model for the origin of teh Yakutat block, an accreting terrane in the northern Gulf of Alaska: Geology, v. 11, no. 12, p. 718-721.

Burbank, D. W., and Anderson, R. S., 2011, Tectonic Geomorphology, 2nd Edition, Wiley-Blackwell.

Burkett, C. A., Bemis, S. P., and Benowitz, J. A., 2016 (in press), Along-fault migration of the Mount McKinley restraining bend of the Denali fault defined by late Quaternary fault patterns and seismicity, Denali National Park and Preserve, Alaska: Tectonophysics.

Chapman, J. B., and al., e., 2008, Neotectonics of the Yakutat collision: Changes in deformation driven by mass redistribution: in Active Tectonics and Seismic Potential of Alaska, Geophysics Monograph Series, edited by J.T. Freumueller, P.J. Haeussler, R. Wesson, and G. Ekstrom,, p. 65-81.

Cooke, M.L., and Murphy, S., 2004, Assessing the work budget and efficiency of fault systems using mechanical models: Journal of Geophysical Research: Solid Earth, v. 109, no. B10, p. 1-13.

Cooke, M.L., and van der Elst, N. J., 2012, Rheologic testing of wet kaolin reveals frictional and bi-viscous behavior typical of crustal materials: Geophysical Research Letters, v. 39.

Cooke, M. L., Schottenfeld, M. T., and Buchanan, S. W., 2013, Evolution of fault efficiency at restraining bends within wet kaolin analog experiments: Journal of Structural Geology, v. 51, p. 180-192.

Crowell, J. C., 1974, Origin of late Cenezoic basins of Southern California: *in* Dickinson, W.R. (ed.), Tectonics and Sedimentation: SEPM Special Publications, v. 22, p. 190-204.

Csejtey, B., Jr., Mullen, M.W., Cox, D.P., and Stricker, G.D., 1992, Geology and geochronology of the Healy quadrangle, south-central Alaska: U.S. Geologic Survey Miscellaneous Investigations Series map I-1961, p. 63, 2 sheets, scale 1:250,000.

Cunningham, W. D., 1995, Orogenesis at the southern tip of the Americas: the structural evolution of the Cordillera Darwin metamorphic complex, southernmost Chile: Tectonophysics, v. 244, p. 197-229.

Cunningham, W. D., and Mann, P., 2007, Tectonics of strike-slip restraining and releasing bends: *in* Cunningham, W.D. and Mann, P. (eds.). Tectonics of strike-slip restraining and releasing bends. Geological Society of London Special Publications, v. 290, p. 1-12.

Dewey, J.F., 1977, Suture zone complexities: A review: Tectonophysics, v. 40, no. 1-2, p. 53-67.

Dolan, J.F., and Haravitch, B.D., 2014, How well do surface slip measurments track slip at depth in large strike-slip earthquakes? The important of fault structural maturity in controlling on-fault slip versus off-fault surface deformation: Eath and Planetary Science Letters, v. 388, p.38-47.

Eastham, K.R., and Ridgway, K.D., 2000, Stratigraphic and Provenance Data from the Upper Jurassic to Upper Cretaceous Kahiltna Assemblage of South-Central Alaska: Studies by the U.S. Geologic Survey in Alaska, 2000, U.S. Geological Survey Professional Paper 1662, p. 45-53.

Eberhart-Phillips, D., Christensen, D. H., Brocher, T. M., Hansen, R., Ruppert, N. A., Haeussler, P. J., and Abers, G. A., 2006, Imaging the transition from Aleutian subduction to Yakutat collision in central Alaska, with local earthquakes and active source data: Journal of Geophysical Research: Solid Earth, v. 111, no. B11, p. B11303.

Engebretson, D., Cox, A., and Gordon, R. C., 1985, Relative motions between oceanic and continental plates in the Pacific Basin: Geological Society of America Special Paper 106, p. 59 p.

England, P., and Molnar, P., 1990, Surfce uplift, uplift of rocks, and exhumation of rocks: Geology, v. 18, p. 1173-1177.

Fitzgerald, P. G., Roeske, S. M., Benowitz, J. A., Riccio, S. J., Perry, S. E., and Armstrong, P. A., 2014, Alternating asymmetric topography of the Alaska range along the strike-slip Denali fault: Strain partitioning and lithospheric control across a terrane suture zone: Tectonics, v. 33, no. 8, p. 1519-1533.

Fitzgerald, P. G., Sorkhabi, R. B., Redfield, T. F., and Stump, E., 1995, Uplift and denudation of the central Alaska Range - a case study in the use of apatite fission-track thermochronology to determine absolute uplift parameters: Journal of Geophysical Research, v. 100 (20), no. 175-20, p. 191.

Fitzgerald, P. G., Stump, E., and Redfield, T. F., 1993, Late Cenozoic uplift of Denali and its relation to relative plate motion and fault morphology: Science, v. 259, no. 5094, p. 497-499.

Haeussler, P. J., 2008, An overview of the neotectonics of interior Alaska: far-field deformation from the Yakutat microplate collision: *in* Freymueller, J.T., Haeussler, P.J., Wesson, R., and Ekstrom, G. eds., Active Tectonics and Seismic Potential of Alaska, Geophysical Monograph Series 179, American Geophysical Union, Washignton, D.C., p. 83-108.

Haeussler, P.J., O'Sullivan, P., Berger, A.L., and Spotila, J.A., 2008, Neogene exhumation of the Tordrillo Mountains, Alaska, and correlations with Denali (Mt. McKinley), *in* Active Tectonics and Seismic Potential of Alaska, Geophysical Monograph Series, edited by J.T. Freymueller, P.J., Haeussler, R. Wesson, and G. Ekstrom, AGU Monograph 179, Washington, D.C., p. 269-285.

Hatem, A. E., Cooke, M. L., and Madden, E. H., 2015, Evolving efficiency of restraining bends within wet kaolin analog experiments Journal of Geophysical Research.

Jadamec, M. A., Magali, I. B., and Roeske, S. M., 2013, Three-dimensional numerical models of flat slab subduction and the Denali fault driving deformation in south-central Alaska: Earth and Planetary Science Letters, v. 376, p. 29-42.

Jones, D. L., Silberling, N. J., Gilbert, W., and Coney, P., 1982, Character, distribution, and tectonic significance of accretionary terranes in central Alaska Range: Journal of Geophysical Research, v. 87, p. 3709-3717.

Karig, D. E., 1979, Material transport with accretionary prisms in the "Knocker" Problem: Journal of Geology, v. 88, p. 27-37.

Lahr, J. C., and Plafker, G., 1980, Holocene Pacific-North American plate interaction in southern Alaska: implications for the Yakataga seismic gap: Geology, v. 8, p. 483-486.

Lease, R.O., Haeussler, P.J., and O'Sullivan, P., 2016, Changing exhumation patterns during Cenozoic growth and glaciation of the Alaska Range: Insights from detrital thermochronology and geochronology: Tectonics, v. 35, no. 4, p. 934-955.

Mann, P., 2007, Global catalogue, classification and tectonic origins of restraining- and releasing bends on active and ancient strike-slip fault systems: *in Cunningham, W.D. and Mann, P. (eds.). Tectonics of strike-slip restraining and releasing bends. Geological Society of London Special Publications*, v. 290, p. 13-142.

McClay, K., and Bonora, M., 2001, Analog models of restraining strepovers in strike-slip fault systems: American Association of Petroleum Geologists Bulletin, v. 85, p. 233-260.

Miller, M.L., Bradlet, D.W., Bundtzen, T.K., and McClelland, W., 2002, Late Cretaceous through Cenozoic Strike-Slip Tectonics of Southwestern Alaska: The Journal of Geology, v. 110, p. 247-270.

Mitra, S., and Paul, D., 2011, Structural geometry adn evolution of releasing and restraining bends: Insights from laser-scanned experimental models: American Association of Petroleum Geologists Bulletin, v. 95, no. 7, p. 1147-1180.

Nokleberg, W. J., J.N., A., Dutro, J., Lanphere, M. A., Silberling, N. J., Silva, S. R., Smith, T. E., and Turner, D. L., 1992, Maps, tables, and summary of fossil and isotopic age data, Mount Hayes quadrangle, eastern Alaska Range, Alaska: U.S. Geological Survey Misc. Invest. Map 1996-3, scale 1:250,000.

Perry, S. E., 2014, Thermotectonic evolution of the eastern Alska Range: constraints from low-temperature thermochronology, PhD Thesis 840 pp., Syracuse University.

Plafker, G., and Berg, H. C., 1994, Overview of the geology and tectonic evolution of Alaska: *in* Plafker, G., and Berg, H.C., eds., The geology of Alaska: Boulder, Colorado, Geological Society of America, Geology of North America, v. G-1, p. 989-1021.

Plafker, G., Naeser, C. W., Zimmerman, R. A., Lull, J. S., and Hudson, T., 1992, Cenezoic uplift history of the Mount McKinley area in the central Alaska Range based on fission track dating: USGS Survey Bulletin, v. 2041, p. 202-212.

Reed, J. C., 1961, Geology of the Mount McKinley quadrangle, Alaska (U.S. Geological Survey Bulletin No. 1108-A).

Reed, B.L., and Nelson, S.W., 1980, Geologic map of the Talkeetna Quadrangle, Alaska: U.S. Geological Survey Miscellaneous Investigations 1174, scale 15 p., 1 sheet, scale 1:250,000, http://www.dggs.alaska.gov/pubs/id/12942

Ridgway, K. D., Trop, J. M., Nokleberg, W. J., Davidson, C. M., and Eastham, K. R., 2002, Mesozoic and Cenozoic tectonics of the eastern and central Alaska Range: Progressive basin development and deformation in a suture zone: Geological Society of America Bulletin, v. 114, no. 12, p. 1480-1504.

Ridgway, K.D., Thoms, E.E., Lesh, M.E., Layer, P.W., White, J.M., and Smith, S.V., 2007, Stratigraphic record and provenance of Neogene foreland basin development, Usibelli Group and Nenana Gravel, Tanan basin, central Alaska Range: *in* Tectonic Growth of a Collisional Continental Magin: Crustal Evolution of Southern Alaska: Geological Society of America Special Paper 431, doi: 10.1130/2007.2431(20).

Roeske, S. M., Snee, L. W., and Pavlis, T. L., 2003, Dextral-slip reactivation of an arc-forearc boundary during Late Cretaceous-early Eocene oblique convergence in the northern Cordillera. *In*: Sisson, V.B., Roeske, S.M., and Pavlis, T.L., (eds) Geology of a Transpressional Orogen Developed During Ridge-Trench Interaction Along the North Pacific Margin.: Geological Society of America, Special Papers, v. 371, p. 141-169.

Small, E.E., and Anderson, R.S., 1995, Geomorphically Driven Late Cenozoic Rock Uplift in the Sierra Nevada, California: Science, v. 270, p. 277-280

Stirling, M.W., Wesnousky, S.G., and Shimazaki, K., 1996, Fault trace complexity, cumulative slip, and the shape of the magnitude-frequency distribution for strike-slip faults: a global study: Geophysical Journal International, v. 124, no. 3, p 833-868

Terhune, P., Benowitz, J.A., Waldien, T.S., Allen, W.K., Davis, K.N., Ridgway, K.D., Roeske, S.M., Fitzgerald, P.G., Brueseke, M.E., O'Sullivan, P.B., 2015, Geochronological framework for the Cenozoic history of the Southern Alaska Range fold and thrust belt: Geological Society of America *Abstracts with Programs*, v. 47, no. 4, p. 60.

Thoms, E.E., 2000, Late Cenozoic unroofing sequence and foreland basin development of the central Alaska Range: Implications from the Nenana Gravel: University of Alaska Fairbanks, M.S. thesis, p. 221.

Thomson, S.N., Brandon, M.T., Tomkin, J.H>, Reiners, P.W., Vásquez, C., and Wilson, N.J., 2010, Glaciation as a destructive and constructive control on mountain building: Nature, v. 467, p. 313-317.

Trop, J. M., Ridgway, K. D., Manuszak, J. D., and Layer, P., 2002, Mesozoic sedimentary-basin development on the allochthonous Wrangellia composite terrane, Wrangell Mountains basin, Alaska: a long-term record of terrane migration and arc construction: Geological Society of America Bulletin, v. 114, no. 6, p. 693-717.

Veenstra, E., Christensen, D.H., Abers, G.A., and Ferris, A., 2006, Crustal thickness variation in south-central Alaska: Geology, v. 34, no. 9, p. 781-784.

Wakabayashi, J., 2007, Stepovers that migrate with respect to affected deposits: field characteristics and speculation on some details of their evolution: Geological Society of London Special Publications 290, p. 169-188.

Ward, D. J., Anderson, R. S., and Haeussler, P. J., 2012, Scaling the Teflon Peaks: Rock type and the generation of extreme relief in the glaciated western Alaska Range: Journal of Geophysical Research, v. 117, no. F1, p. 1-20.

Wesnousky, S.G., 1998, Seismological and structural evolution of strike-slip faults: Nature, v. 335, p. 340-343.

Whipple, K., Kirby, E., and Brocklehurt, S., 1999, Geomorphic limits on climatically induced increases in topographic relief: Nature, v. 401, p. 39-43.

Wilson, F. H., J.H., D., Bradley, D. C., Weber, F. R., Bundtzen, T. K., and Haeussler, P. J., 1998, Geologic map of central (interior) Alaska (Open-File Report No. 98-133-A). U.S. Geologic Survey.

VITA

Anne Margaret Fendick
Sacramento, California

Education:
Bachelor of Arts with Honors, Geology, Occidental College, Los Angeles, California 2014

Professional Positions:

- Analyst, Quantum Spatial, Lexington, Kentucky, present
- Geology Intern, Occidental Petroleum, Long Beach, California 2014

Professional Publications:

- Fendick, A., Bemis, S., Toeneboehn, K., Cooke, M., Benowitz, J., Denali in a box: analog experiments modeled after a natural setting provide insight on gentle restraining bend deformation, EGU2016-10996; European Geosciences Union, General Assembly, Vienna, Austria, April 2016
- Fendick, A.M., Blythe, A.E., DiBiase, R.A., Refining block uplift and exhumation of the San Gabriel Mountains, CA, using low-temperature thermochronology, Paper No. 307-10; Geological Society of America, Annual Meeting, Denver, CO, October 2013
- Chinn, L., Blythe, A.E., Fendick, A.M., Quantifying vertical exhumation in Intracontinental Strike-Slip Faults: The Garlock fault zone, southern California, Abstract No. T33F-2717; American Geophysical Union, Fall Meeting, San Francisco, CA, December 2012